OPEN ACCESS Freely available online

Kinetics of Rhodopsin Deactivation and Its Role in Regulating Recovery and Reproducibility of Rod Photoresponse

Giovanni Caruso[1], Paolo Bisegna[2], Leonardo Lenoci[3], Daniele Andreucci[4], Vsevolod V. Gurevich[3], Heidi E. Hamm[3], Emmanuele DiBenedetto[5]*

1 Construction Technologies Institute, National Research Council, Rome, Italy, **2** Department of Civil Engineering, University of Rome Tor Vergata, Rome, Italy, **3** Department of Pharmacology, Vanderbilt University Medical Center, Nashville, Tennessee, United States of America, **4** Department of Mathematical Methods and Models, University of Rome La Sapienza, Rome, Italy, **5** Department of Mathematics, Vanderbilt University, Nashville, Tennessee, United States of America

Abstract

The single photon response (SPR) in vertebrate phototransduction is regulated by the dynamics of R^* during its lifetime, including the random number of phosphorylations, the catalytic activity and the random sojourn time at each phosphorylation level. Because of this randomness the electrical responses are expected to be inherently variable. However the SPR is highly reproducible. The mechanisms that confer to the SPR such a low variability are not completely understood. The kinetics of rhodopsin deactivation is investigated by a Continuous Time Markov Chain (CTMC) based on the biochemistry of rhodopsin activation and deactivation, interfaced with a spatio-temporal model of phototransduction. The model parameters are extracted from the photoresponse data of both wild type and mutant mice, having variable numbers of phosphorylation sites and, with the same set of parameters, the model reproduces both WT and mutant responses. The sources of variability are dissected into its components, by asking whether a random number of turnoff steps, a random sojourn time between steps, or both, give rise to the known variability. The model shows that only the randomness of the sojourn times in each of the phosphorylated states contributes to the Coefficient of Variation (CV) of the response, whereas the randomness of the number of R^* turnoff steps has a negligible effect. These results counter the view that the larger the number of decay steps of R^*, the more stable the photoresponse is. Our results indicate that R^* shutoff is responsible for the variability of the photoresponse, while the diffusion of the second messengers acts as a variability suppressor.

Citation: Caruso G, Bisegna P, Lenoci L, Andreucci D, Gurevich VV, et al. (2010) Kinetics of Rhodopsin Deactivation and Its Role in Regulating Recovery and Reproducibility of Rod Photoresponse. PLoS Comput Biol 6(12): e1001031. doi:10.1371/journal.pcbi.1001031

Editor: Rama Ranganathan, UT Southwestern Medical Center, United States of America

Received April 28, 2010; **Accepted** November 11, 2010; **Published** December 16, 2010

Funding: This work was supported by NIH grants EY011500(VVG), 1RO1GM068953(ED), EY006062(HEH) and NSF-DMS 0652385. The funders had no role in study design, data collection and analysis, decision to publish, or preparation of the manuscript.

Competing Interests: The authors have declared that no competing interests exist.

* E-mail: em.diben@vanderbilt.edu

Introduction

In retinal rod photoreceptors, rhodopsin activated by photons of light, denoted by R^*, initiates a signal transduction cascade to produce a suppression of electrical current flowing into rod outer segment (ROS). Following isomerization, a molecule R^* undergoes a random number of phosphorylations by rhodopsin kinase (RK) and finally is inactivated by arrestin (Arr) binding. Activated rhodopsin R^*, moving along its random path, during its random lifetime from isomerization to Arr binding, keeps activating its cognate G-protein (G) transducin, while its catalytic activity declines with increasing level of phosphorylation. The active G-protein (G^*) associates with the effector protein phosphodiesterase (E) forming an active G^*-E^* complex, which by hydrolyzing cGMP reduces its concentration, thereby generating a current response on the outer shell of the ROS. The dynamics of R^* during its lifetime, including the random number of phosphorylations, the catalytic activity and the random sojourn time at each phosphorylation level, regulates the production of G^* and therefore the current response. Because of the randomness in the components of the activation/deactivation cascade, the electrical responses are expected to be inherently variable. However, the single photon response (SPR) exhibits a low variability in the sense that the amplitude and shape of the electrical responses, corresponding to a set of activation-deactivation events, are similar. It is reported that the Coefficient of Variation (CV = standard deviation/mean) of the SPR area for mouse is about 36% [1]. However, the mechanisms that confer high reproducibility of the SPR are not completely understood.

Several studies [1–7] attribute the high reproducibility of the SPR mainly to the mechanisms regulating rhodopsin deactivation. Although the models proposed in these studies account for the low variability of the response, they impose, in one way or another, certain restrictions on the biochemistry of rhodopsin deactivation. For example, if rhodopsin's integrated activity occurs in k independent steps, it is assumed that each step controls an equal fraction of rhodopsin's integrated catalytic activity [1,2]. It is then natural to ask what is the statistical mean N of the number k, as a way of testing both the models and the supporting biochemical

Author Summary

Reception and transmission of biological stimuli such as vision, olfaction, taste, and hormone and neurotransmitter signal transduction, contain inherently variable components. Yet, biological functions are stable and reliable. For each signaling process, it is of interest to investigate the causes of variability and the mechanisms by which variability is mitigated to yield responses that reliably reflect the strength of the stimulus. We have investigated the variability of the single photon response in rod photoreceptors. A photon of light is captured by a receptor rhodopsin, and it goes through a series of biochemical states ending with a random shutoff. We have created a mathematical model of such a process, based on the recent biochemical findings on activation/deactivation, capable of reproducing the peculiar experimental features of visual trasduction both in wild type and genetically modified mice. We have found that the randomness of the time that rhodopsin sojourns in each of these biochemical states is the dominant cause of variability, whereas diffusion of molecules carrying the signal within the cell acts as variability mitigators.

assumptions. Mechanistically, one might ask which of the components of the deactivation cascade contribute more importantly to the variability.

A major difficulty with these issues is to experimentally separate the various components that contribute to the variability. To our knowledge, the activation/deactivation module of the cascade is not, to date, experimentally separable from the transduction module. We have shown in [8] that diffusion of the second messengers in the cytoplasm acts as a variability suppressor. The separation between the activation cascade on the disks and the diffusion of the second messengers cGMP and Ca^{2+} in the cytoplasm is realized by a mathematical model [8–11]. Likewise several fine properties of the biochemical and biophysical mechanisms regulating the recovery and reproducibility of SPR are not, to our knowledge, experimentally separable. Here we attempted to tease apart the various components of the R^* shutoff mechanism and analyze to what extent each of them contributes to the variability of the SPR. Unlike the transduction part of the cascade, where the intricacy is of geometrical nature [9–11], the main difficulty here is stochastic. Rhodopsin inactivation can occur by several mechanisms, including Arr binding and thermal decay to opsin. We only model the former, as the latter occurs on a much longer time scale [12,13]. Shutoff of R^* by Arr binding can follow, in principle, an infinite number of paths, depending on the random number of phosphorylated states, and the random sojourn times in those states.

The biochemistry that regulates rhodopsin deactivation is put into a stochastic framework, which reproduces the SPR both in WT and in mutant mice, and is capable of analyzing the randomness of each phosphorylation state of R^*. This is interfaced with the spatio-temporal model in [8,9,11], capable of tracking the diffusion of the second messengers in the cytoplasm and of detecting the effects of geometrical changes of the ROS on the photoresponse.

We find that the randomness of the sojourn times of R^* in each of its phosphorylation states acts as the dominant factor contributing to the CV of the response. At the same time the number of available phosphorylation sites or the random number of R^* phosphorylations before shutoff, is shown to contribute little to variability suppression.

We also find that, in addition to changed biochemistry, the geometry of the ROS might be important for the light response in mutant mice.

Results

The technical aspects of the mathematical model are presented in **Methods**. Here we illustrate the main links between statistics, biochemistry and geometry. Label by the integer i the state at which activated rhodopsin R^* has acquired $(i-1)$ phosphates. Thus for example if $i=4$ then R^* has acquired 3 phosphates. Then either R^* can acquire a further phosphate at a rate λ_i (determined by RK phosphorylation rate), or it can be quenched by Arr at a rate μ_i (determined by Arr on-rate). While in the $i-\text{th}$ state, R^* activates G protein with catalytic activity ν_i. Finally R^* remains in the $i-\text{th}$ state a random sojourn time s_i, of mean τ_i. This is a typical sequence of Bernoulli trials whose statistical description by a Continuous Time Markov Chain (CTMC) is well known and standard [2,14–16].

The main point of the model is in introducing a theoretical scheme that identifies the parameters of each of these steps in terms of their biochemical role. It turns out that WT responses alone are not sufficient to identify the parameters $\{\lambda_i,\mu_i,\tau_i,\nu_i\}$. They are identified using recent experimental data obtained in genetically modified mice ([17–20]).

When these parameters are identified, the CTMC translates the deactivation cascade into the probabilities $P_i(t)$ for rhodopsin to be in the $i-\text{th}$ state at time t. The output of the activation/deactivation cascade, computed by this CTMC scheme, and measured in terms of activated effector E^*, is then used as input in the spatio-temporal model introduced in [8–11]. The latter describes the dynamics of the second messengers cGMP and Ca^{2+} in the cytoplasm of the ROS, and the generation of photocurrent $j_{tot}(t)$ flowing through the cell membrane of the ROS, as a function of time t. These two modules, so interfaced, provide a systems approach to phototransduction by mathematically separating, and then blending, the random events of the activation cascade occurring on a disk, the diffusion of second messengers in the cytoplasm, and current suppression on the outer shell.

The variability of the effector E^* is described by the following functionals:

$$
\begin{array}{ll}
E^*(t) & \text{total number of molecules of } E^* \text{ in } D_{\text{eff}} \text{ at time } t \\
E^*_{\text{int}}(t)=\int_0^t E^*(s)ds & \text{total activity of } E^* \text{ up to time } t \\
E^*_{\text{area}}=\int_0^\infty E^*(t)dt & \text{total activity of } E^* \text{ over the entire lifetime of the process} \\
E^*\left(t^*_{\text{peak}}\right) & \text{peak value of } E^*(t).
\end{array}
\qquad (1)
$$

The last two are scalar quantities and their CV is reported in Table 1. The first two are functions of time. The CV of the second, as a function of time is reported in Figure 1 (left). The natural variable functionals of the photocurrent are

Table 1. Coefficients of variation, $\tau_{R;eff} \approx 75$ ms.

Sites		0P	1P	2P	3P	4P	5P	6P(WT)
$E^*\left(t^*_{peak}\right)$	**Case1**	0.00	0.12	0.21	0.35	0.40	0.44	0.46
	Case2	0.00	0.00	0.00	0.00	0.00	0.00	0.00
	Case3	0.00	0.12	0.21	0.35	0.40	0.43	0.45
E^*_{area}	**Case1**	0.00	0.02	0.03	0.57	0.56	0.57	0.57
	Case2	0.00	0.00	0.00	0.00	0.02	0.02	0.03
	Case3	0.00	0.02	0.03	0.57	0.56	0.56	0.55
$^{(teor)}E^*_{area}$	**Case1**	-	-	-	0.56	0.54	0.52	0.51
$I(t_{peak})$	**Case1**	0.00	0.04	0.07	0.16	0.23	0.27	0.30
	Case2	0.00	0.00	0.00	0.00	0.00	0.01	0.01
	Case3	0.00	0.04	0.07	0.17	0.22	0.26	0.29
I_{area}	**Case1**	0.00	0.01	0.01	0.37	0.36	0.37	0.38
	Case2	0.00	0.00	0.00	0.00	0.01	0.02	0.02
	Case3	0.00	0.01	0.01	0.38	0.36	0.37	0.37

CV (σ/μ) calculated for a 3 s simulation and 5000 trials for each of **Case 1**: Fixed number of steps to R^* shutoff and random sojourn times s_i; **Case 2**: Fixed sojourn times s_i and random number of steps to R^*; **Case 3**: Both sojourn times s_i and R^* shutoff steps are random. The parameters τ_{R^*} and $\tau_{R;eff}$ and their equivalence for WT mouse are discussed in the section § **Parameters**. The theoretical values of $^{(teor)}E^*_{area}$ are reported for 3-6P as the theoretical formula of Eq:3-Eq:4 is valid only for these cases.

doi:10.1371/journal.pcbi.1001031.t001

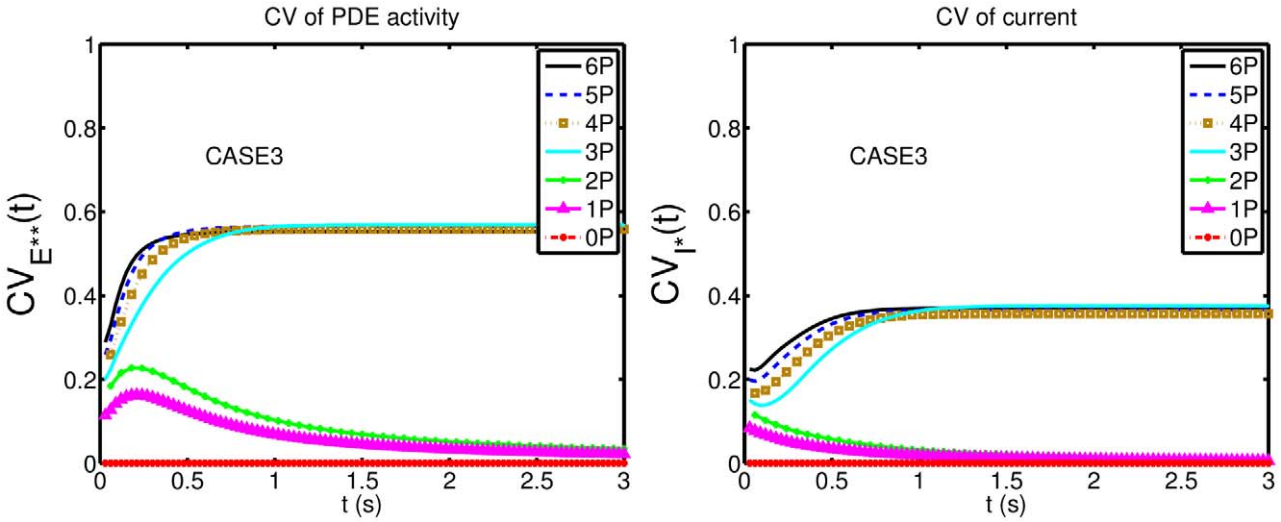

Figure 1. Comparing the CVs of the total activated effectors $E^*_{int}(t) = \int_0^t E^*(s)ds$ at time t with the CVs of the total relative charge $I_{int}(t) = \int_0^t I(s)ds$ up to time t. All simulations assume both the sojourn time and the number of R^* shutoff steps as random (Case 3 of Test Cases). The CVs of both $E^*_{int}(t)$ and $I_{int}(t)$ stabilize asymptotically for three or more phosphorylation sites (3P–6P). A CV of about 60% for $E^*_{int}(t)$ at times past the peak time is reduced to a CV of about 40% for the corresponding photocurrent $I_{int}(t)$. This points to an intrinsic variability reduction effect of the diffusion part of the process.

doi:10.1371/journal.pcbi.1001031.g001

$$\begin{aligned}
&I(t)=1-\frac{j_{tot}(t)}{j_{dark}} && \text{total (relative) current sup pression at time } t\\
&I_{int}(t)=\int_0^t I(s)ds && \text{total (relative) charge suppression up to time } t \qquad (2)\\
&I_{area}=\int_0^\infty I(t)dt && \text{total (relative) charge suppression over the time course of the phenomenon}\\
&I(t_{peak}) && \text{peak value of } I(t).
\end{aligned}$$

While the last one is the value of the first at peak time, we have listed it separately since it is frequently reported in the literature [5,6,21]. $I(t_{peak})$ is a scalar quantity and its CV is tabulated in Table 1. The first two are functions of time. The CV of the second is graphed as a function of t in Figure 1 (right). The quantity I_{area} is the total relative charge produced over the entire time course of the phenomenon following isomerization by a single photon and is referred to as the SPR area [1,2,4,22].

Simulating the SPR in Transgenic Mice

Deactivation of rhodopsin with one or several mutant phosphorylation sites, can be simulated by suitable choices of the sequences $\{\lambda_i\}$ and $\{\mu_i\}$ as indicated in the section of numerical procedures and methods.

Mutant mouse rhodopsins bearing fewer than 6 phosphorylation sites generate SPRs of significantly extended durations (Figure 2A). The rate of recovery increases with increasing numbers of phosphorylation sites (Figure 2A), in qualitative and quantitative agreement with the experimental results of [3] (Figure 2B).

Inactivation of all rhodopsin phosphorylation sites is realized by either mutation of all six serines and threonines to alanines [1,3], or rhodopsin kinase knockout [23]. The corresponding SPRs are similar, exhibiting larger amplitude and longer duration than WT (Figure 2B,D for (0P)).

A prolonged SPR in mutant mouse rods lacking arrestin is reported in [24] (Figure 2D). This is realized by setting $\mu_i=0$ for all $i=0,1,\ldots,6$ in the model. The activated rhodopsin gets phosphorylated until all six sites are occupied. Its activity is reduced with increased phosphorylations, and kept fixed after the last phosphorylation for the remainder of the process. The remaining activity yields a response with an asymptotic tail at almost half of its peak value. The initial fall of the response is triggered by phosphorylation. The simulations are shown by (–/–) in Figure 2C, and are qualitatively and quantitatively in agreement with the experimental studies of [24] (Figure 2D).

In Table 2 we report the simulated characteristics of SPRs from WT rods and those expressing rhodopsin mutants. By increasing the number of phosphorylation sites, the peaks of the current response $I(t_{peak})$ decrease; the time to peak t_{peak} decreases; and the SPR area I_{area} decreases significantly. For mutants that exhibit very slow recovery (0P, 1P, 2P) the corresponding I_{area} is large because the current remains high for an extended period of time. The value of I_{area} has been computed by integrating the photocurrent over the time of simulation (3s).

When only one phosphorylation site was mutated, the SPR was almost like that of WT but recovery was slightly slower. Consistent with this slower recovery, the SPR area I_{area} of the response of rhodopsin with five phosphorylation sites (5P) was about 14% larger than those for wild type. Taken together, these results are consistent with the experimental observations of [3] and the notion that normal kinetics of R^* deactivation requires the presence of all six phosphorylation sites.

We finally comment on the largest rising curves coded in red in Figure 2B and D. Various experimental studies [3,23] show that the response amplitude for the case (0P) is roughly twice as large as the response for the case (1P). In [3] the case (0P), is realized by CSM, and in [23] by RK knockout. In both cases all phosphorylation sites are removed or made inoperative, and both cases exhibit the double amplitude response, suggesting a common mechanism. This issue is not discussed in the indicated papers and we are not aware of an explanation or hypothesis for a possible biochemical mechanism. However, Figure 2 of [3] shows that the ROS in CSM mice were about 25% shorter than WT. Geometrical changes due to genetic manipulations are also discussed in [23] (page 3720), and [24], (Figure 3d, page 506). We repeated the simulations with a ROS whose height H was reduced by 30%, while all the remaining parameters were kept fixed. In particular, the number of channels was kept fixed, thereby increasing their density. Since the response is localized close to the activation site [10,11], the augmented channel density yields a larger response. The resulting simulation is reported in Figure 2A for (0P*) as the largest amplitude (red curve). While the agreement with corresponding experimental curve in Figure 2B is striking, at this point we refrain from suggesting that this as the only functional mechanism.

Variability

The CTMC model permits one to test independently the effects of the random components of the variability on the response. For example one can separate the effects of the randomness of the sojourn time from the randomness of number of shutoff steps. To achieve this, we performed the following sets of simulations:

- **Case 1**. Fix the number of steps to R^* shutoff at that integer closest to its mean N, and let R^* have random sojourn time s_i at the corresponding state. The random numbers s_i are generated according to their exponential distribution with mean τ_i.
- **Case 2**. Fix the sojourn times of R^* at their mean τ_i and let R^* be shut off in k random steps. The random number k of R^* shutoff steps is generated by a series of Bernoulli trails, in which the probability of phosphorylation is $\frac{\lambda_i}{\lambda_i+\mu_i}$ and the probability of Arr binding is $\frac{\mu_i}{\lambda_i+\mu_i}$. Thus the mean N of the random number k is computed from Eq:10–Eq:11.
- **Case 3**. Both sojourn time s_i and the number of shutoff steps k are random. This is the biologically realistic case, although the previous cases extract the effect of the randomness of each component on the variability of the response.

Stochastic simulations are effected for WT and each of the knock-out cases of COOH-terminal truncations [24,25] and RK knockout [1,3]. After about 5,000 numerical simulations, up to 3 s, mean, standard deviation and CV are computed for effector and normalized current suppression. Further technical details are in **Methods**.

Variability of E^*. The first two lines of Table 1 report the CV of the scalar quantities E^*_{area}, and $E^*(t_{peak})$ defined in Eq:1, and for R^* bearing $i=0,1,\ldots,6$ phosphorylation sites. The first

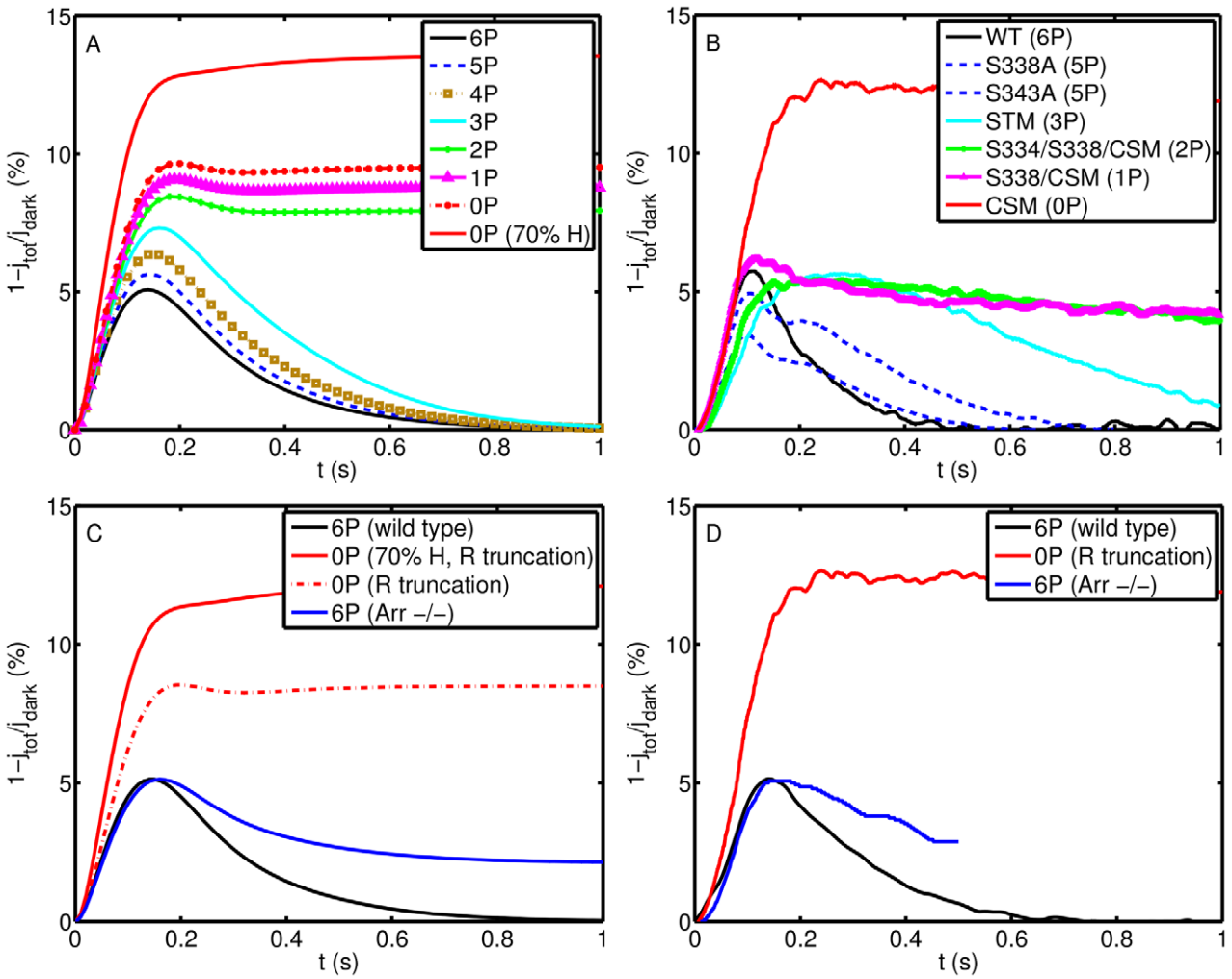

Figure 2. Simulations SPR for mutant phosphorylation sites of R^*, or with Arr knockout. Panel A: Simulated SPRs for rhodopsin with a number $n=0,1,\ldots,6$ of available phosphorylation sites (thus $(6-n)$ sites are mutant); **Panel B**: Reproduction of data from [3] showing SPRs from mutant mice with different phosphorylation sites. CSM: completely substituted mutant (0P); STM: serine triple mutant (3P); S338A: mutant lacking S338 (5P); S343A: mutant lacking residue S343 (5P); S338/CSM: one site (S338) was restored in the CSM (1P); S334/S338/CSM: two sites (S334 and S338) were restored in the CSM (2P); Mutant rhodopsins bearing zero, one (S338), or two (S334/S338) phosphorylation sites generated single-photon responses with greatly prolonged durations. Responses from rods expressing mutant rhodopsins bearing more than two phosphorylation sites declined along smooth, reproducible time courses; the rate of recovery increased with increasing numbers of phosphorylation sites; **Panel C**: Simulated SPRs with no phosphorylation site (0P), lacking arrestin (–/–), and wild type (WT); **Panel D**: Reproduction of the SPRs from rod with C terminal truncation, lacking arrestin (–/–), and wild type (+/+) [24] rescaled to exhibit the same proportional amplitude as the wild type SPR. The simulated curves were rescaled accordingly. With arrestin absent, the flash response displayed a rapid partial recovery followed by a prolonged final phase. This behavior indicates that an arrestin-independent mechanism initiates the quench of rhodopsin's catalytic activity and that arrestin completes the quench. Analogous simulations for the faster dynamics $\tau_{R;eff}\approx 40$ ms and $\nu_{RG}\approx 575 s^{-1}$ are in Figure S2 of the supplementary material.
doi:10.1371/journal.pcbi.1001031.g002

Table 2. Characteristics of SPRs, $\tau_{R;eff}\approx 75$ ms and $\tau_{R;eff}\approx 40$ ms.

	Rhodopsin	0P	1P	2P	3P	4P	5P	6P(WT)
$\tau_{R;eff}\approx 75$ **ms**	$I(t_{peak})$	**8.54**	**8.02**	**7.50**	**6.83**	**6.19**	**5.62**	**5.13**
	t_{peak} (s)	0.20	0.19	0.19	0.17	0.16	0.15	0.14
	I_{area} (s)	24.81	22.35	19.60	2.89	2.11	1.74	1.51
$\tau_{R;eff}\approx 40$ **ms**	$I(t_{peak})$	**9.66**	**9.08**	**8.47**	**7.32**	**6.38**	**5.65**	**5.08**
	t_{peak} (s)	0.19	0.19	0.19	0.16	0.15	0.14	0.14
	I_{area} (s)	27.86	25.74	23.34	2.73	2.07	1.74	1.52

Characteristics of SPRs from Wild Type and Rhodopsin Mutant Rods from 3 s simulations for the dynamics $\tau_{R;eff}\approx 75$ms and $\nu_{RG}\approx 330 s^{-1}$ and $\tau_{R;eff}\approx 40$ms and $\nu_{RG}\approx 575 s^{-1}$. The parameters τ_{R^*} and $\tau_{R;eff}$ and their equivalence are discussed in § **Parameters**.
doi:10.1371/journal.pcbi.1001031.t002

result is that the CV for **Case 2** is negligible (computationally up to 2 decimal points). This indicates that the randomness of the number of R^* shutoff steps does not significantly contribute to the CV of E^*. The second result is that the CVs produced by **Case 1**, to which only the randomness of sojourn time of R^* contributes, are roughly the same as those of **Case 3**, where all components are allowed to be random. It appears from the table that the randomness of the sojourn times of R^* in its phosphorylated states is largely responsible for the CV of E^* in this model.

For mutant R^* with zero phosphorylation sites (0P), the CV of any of these quantities is zero in all cases. Since R^* could neither be phosphorylated nor be bound by Arr ($N=0$), it remains in state 1 indefinitely and the process has no random components, within the time scale of the simulation. On a longer time scale, eventually active metarhodopsin II releases bound all-trans-retinal and decays to opsin, losing most of its ability to activate transducin. It is not surprising that R^* with deactivation deficit leads to a highly reproducible SPR in the very first few seconds (3 s in our simulations), as no inactivation occurs.

The observations in [1] (see Figure 3, Panel F of [1]), indicate that the SPRs generated by unphosphorylated R^* are highly reproducible within the very first few seconds (about 10s). Later shutoff of unphosphorylated R^* is believed to be due to thermal decay of R^* to opsin [12]. Here we are interested in the deactivation of R^* within the time scale of normal SPR (3 s in our simulations) and the effects that could be involved beyond this time period are not considered.

For mutant R^* with one phosphorylation site (1P, $n=2$), the CV of any one of the variability functionals in Eq:1–Eq:2 is very small. Such a mutant R^* could be phosphorylated to one level, but it could not be shut off by Arr binding since mono-phosphorylated R^* has the same low Arr binding levels as unphosphorylated R^* (see the discussion in **Methods** and [20]). The randomness of one extra level of phosphorylation causes a noticeable increase in uncertainty as measured by the CVs. From Eq:7–Eq:11 one computes $\tau_1=\lambda_o^{-1}$ and $\tau_2=\infty$. Therefore R^* remains in the unphosphorylated state 1, for a random sojourn time s_1 of mean λ_o^{-1}; then it transitions to state 2 by acquiring a phosphate and it remains indefinitely in that state. The only randomness is due to the sojourn time s_1, which affects the CV of $E^*\left(t^*_{peak}\right)$. Since R^* is never turned off (within the 3 s time frame used here), the functional E^*_{area}, is uniformly large for all trials, and therefore it exhibits negligible variability.

Compared with the CV of 1P, the mutant R^* with two phosphorylation sites (2P, $n=3$) exhibits a larger CV for any of the variability functionals, the increase in uncertainty being due to the second phosphorylation site. The only randomness of the process is due to sojourn times s_j of means τ_j, as the number of possible steps ($k=N=3$) is not random. In the case of 2P the uncertainty of s_3 is compounded, with respect to the case 1P, by the uncertainty of the random sojourn times s_1 and s_2, although their mean is smaller. Accordingly all functionals exhibit larger variability. Also for the case 2P shutoff does not occur since $\tau_3=\infty$ (from Eq:7–Eq:9). Therefore, for the cases 0P, 1P and 2P, the CVs of the functionals E^*_{area} and I_{area} reported in Table 1 is not due to variations caused by inactivation, as the latter, theoretically, never occurs. In reality, inactivation does occur, although by different mechanisms, for example thermal decay to opsin, on a much larger time scale.

As the number of available phosphorylation sites increases ($n-1=3,\ldots,6$), one might expect that the uncertainty of the sojourn times s_j, be compounded by the randomness of the number of steps $k\in\{4,\ldots,7\}$ to R^* shutoff. However Table 1 shows no significant difference in the CV of all functionals, between Case 1, where the number of steps to R^* shutoff is kept fixed to its mean N, and Case 3, where all components are permitted to be random. This suggests that the behavior of the various CVs reflects the randomness of the sojourn times.

For $k\geq 4$ fixed at its mean N (**Case 1**), the CV of E^*_{area} is computed by the explicit formula [8]

$$\mathrm{CV}\left(E^*_{area}\right)=\frac{\sqrt{\sum_{j=1}^{N}\left(\nu_j\tau_j\right)^2}}{\sum_{j=1}^{N}\nu_j\tau_j}. \quad (3)$$

This formula is valid provided

$$0<\nu_i\tau_i<\infty \text{ for all } i=1,\ldots,N, \text{ and if } E^*(\infty)=E^*(0)=0. \quad (4)$$

The latter condition stipulates that the system returns to its original dark state after a sufficiently large time. Therefore this formula holds true only for the cases 3P-6P.

For **Case 1**, with the number of steps to shutoff fixed at the closest integer to the mean N, we have computed explicitly the sequences $\{\nu_j\}$ and $\{\tau_j\}$ from Eq:7–Eq:9 and have computed the corresponding CV from formula Eq:3. These theoretical CVs are reported in line 7 of Table 1 and show a reasonably good agreement with the simulated values of $\mathrm{CV}(E^*_{area})$.

In Figure 1 (left), we report the graphs of the CV for $E^*_{int}(t)$ as function of time, only for Case 3. Indeed, this is the biologically realistic case, where all the components of the phenomenon are permitted to be random. This variability functional is defined in Eq:1. Similarly as observed in the context of Table 1, the CV for 0P is negligible and the CV of 1P and 2P are relatively small.

The CV of $E^*_{int}(t)$, for wild type (6P), stabilizes from 0.90 s with a value of 0.55, and the CV of the same functional for 3P, stabilizes from 1.41 s with a value of 0.57. By increasing the number of phosphorylation sites from 3P to 6P, the stabilized CVs of the functional E^*_{area} decrease (Table 1), and the time at which the CVs begins to stabilize decreases.

The functional E^*_{area} compounds the variability of the process at all times, up to recovery, and therefore its CV is expected to be larger than the CV of $E^*\left(t^*_{peak}\right)$.

Variability of the photocurrent. In the last two rows of Table 1 we have reported the CV of the scalar quantities $I\left(t_{peak}\right)$ and I_{area}, defined in Eq:2, for each of the **Test Cases 1,2,3**, and for a R^* bearing $j=0,1,\ldots,6$ phosphorylation sites. The results exhibit a pattern similar to the CVs of E^* and $E^*\left(t^*_{peak}\right)$ although at considerably lower values of CV. A CV of about 55% for E^*_{area} is reduced to a CV of about 37% for the corresponding photocurrent I_{area}. Thus the diffusion part of the process acts as variability suppressor, in agreement with the results of [8].

The simulations show that CV of I_{area} is essentially constant with respect to the number of available phosphorylation sites 3–6.

Figure 1 (right) reports the CV of the total relative charge $I_{int}(t)$ produced up to time t, for the physically realistic Case 3, where all random components are present. The results exhibit a pattern similar to those in the left panel of the CV for $E^*_{int}(t)$ although, again, at considerably lower values of CV. The CV of 0P is zero and the CV of 1P and 2P is relatively small. For R^* with three or more phosphorylation sites, the CV increases with increasing phosphorylation sites, at the early times of the activation. Thereafter, the CVs for different number of phosphorylation sites tends to stabilize with stabilization time inversely proportional to the number of available sites, i.e., the more sites R^* has, the faster CV stabilizes.

Discussion

Variability of the photoresponse hinges on a coordinated system behavior of several components. The main two modules are the activation/deactivation part and the transduction part of the cascade. The latter, given its input, is essentially deterministic as it involves the diffusion of the second messengers cGMP and Ca^{2+} in the cytoplasm and a subsequent current drop through the closure of the cGMP -gated channels. The former is essentially stochastic as it involves the biochemistry of rhodopsin shutoff, which occurs in several random steps. An understanding of the process hinges upon teasing apart all these components, analyzing them separately and blending them together into a system behavior. This point of view began in [8], by separating the role of the transduction from that of the activation/deactivation. This separation was made possible by a mathematical model capable of distinguishing the biochemistry of R^* shutoff, from the functional role of the transduction [8,9,11]. A surprising finding was that, while R^* shutoff is responsible for the variability of the photoresponse, the diffusion of the second messengers acts as a variability suppressor.

Here we have further separated the various steps of the deactivation cascade by (a) prescribing a probabilistic mechanism (CTMC) by which the system selects its random states, and (b) by interrogating the known biochemistry to trace patterns and parameters.

It is not sufficient to determine these parameters unambiguously using WT mice. Experimental information from some mutant and knock-out animals is needed. Specifically, the choice of the catalytic activities v_i by formula Eq:6, while based on known biochemistry [26], hinges upon the basic parameter k_v, which in turn is determined by the biochemistry of the cascade in mutant mouse (section on parameters in **Methods**). The same holds true for the transition parameters λ_i, given by formula Eq:7 and depending upon the parameter λ_o. Thus, a first remark is that our approach, while mathematical and computational, parallels the biology; that is, information is extracted in a complementary way from the data on genetically modified as well as WT animals. Next the model populated by the indicated parameters is validated against WT and mutant responses as in Figure 2. The model has a deterministic component, and a stochastic component. The first regards the transduction part of the cascade, which is geometry dependent, and deterministic, being based on the diffusion of the second messengers cGMP and Ca^{2+} in the cytoplasm.

Importantly, this model permits one to test the response against geometrical variations of the ROS. The response in mice expressing CSM or RK knock out is rather unusual, exhibiting a double amplitude with respect to WT [3,23]. An examination of the immunofluorescence micrographs in Figure 2 of [3], suggests that the length of ROS in CSM mice is reduced by about 25% relative to WT. Geometrical modifications presumably due to genetic manipulations are also discussed in [23]. Keeping the same stochastic biochemical scheme and changing the length of the ROS, the model reproduced the double-amplitude phenomenon described in [3,23] (Figure 2 A,B), suggesting that the modified geometry of mutant ROS, might contribute, along with the changed biochemistry, to this phenomenon. This results, along with a recent study of rod signaling in mice expressing supraphysiological levels of rhodopsin ([27]), emphasize the importance of investigating the ROS geometry in genetically modified mouse lines. Our analysis shows that the changes in ROS length, which were analyzed in very few mouse lines, can have dramatic effects on photoresponse.

The stochastic component permits one to single out those parts of the activation/deactivation cascade that dominantly contribute to the variability of the response. The main result is that variability is largely generated by the randomness of the sojourn times of R^* in its phosphorylation states. The prevailing point of view is that the activation cascade is responsible for the variability, although in a non quantified way, and that deactivation of R^* is responsible for variability suppression, and further, the larger the number of decay steps of R^*, the more stable the photoresponse [1,3–7]. This view was expressed in [1], where mice expressing rhodopsin with 0,1,2,5, and 6 phosphorylation sites were used. The analysis presented in [1] has some inconsistencies. Although the experimental points seem to be best fitted by a straight line (Figure 1 of [1]) the authors describe them by $f(N_p)=1/\sqrt{N_p+1}$, with N_p being the number of available phosphorylation sites. The lines with 3 and 4 phosphorylation sites, which would have allowed to discriminate between these functions, were not analyzed in [1]. In addition, by comparing the CV of mice with 0,1, and 2 sites, which do not demonstrate rapid recovery ([4]), with those having 5 or 6 (WT) sites that recover with essentially the same fast rate, the authors inappropriately lump together two disparate phenomena. In the latter case, normal two-step rhodopsin inactivation by RK phosphorylation and arrestin binding is fully operative, whereas in the former rhodopsin is inactivated by stochastic thermal decay taking place on a much longer time course. The idea that multiple inactivation steps are necessary to suppress variability was recently expressed in [2], where the authors conclusions were largely based on two assumptions. The first is that R^* activity is nearly equally distributed among the deactivation steps. The second is that in Ames' solution, that yields much greater and longer-lasting SPR than Locke's ([2,28]), rhodopsin inactivation is rate-limiting and dominates the recovery kinetics. The biochemical scheme we propose argues against the first assumption, on experimental grounds (see a discussion below and **On the Parameters τ_{R^*} and $\tau_{R;eff}$**). The second assumption has been recently questioned in [28], where the authors showed that RGS9 overexpression similarly accelerates the recovery measures in Locke's and Ames' solutions, indicating that transducin inactivation is rate limiting in both cases. Additional issues with data analysis of [1] were discussed in [28]. Thus, no compelling experimental evidence that the number of inactivation steps reduces variability can be found in the literature.

Our results offer a different perspective; demonstrating that variability is generated by the randomness of the sojourn times of R^* in its phosphorylated states, and that increasing the number of these states does not lead to variability suppression.

The number of steps to deactivation does not coincide with the number of available phosphorylation sites. The experimental studies of [20] suggest that one phosphorylation is not sufficient for Arr binding, and the probability of quenching becomes large after 3 phosphorylations. Specifically $0P$ corresponds to $n=1$ by which Eq:7–Eq:8 give $\lambda_1=\mu_1=0$ and hence $\tau_1=\infty$ by Eq:9. Thus, the system remains indefinitely activated (in reality it is stochastically inactivated by the thermal decay of rhodopsin, which is too slow to be captured by 3 s simulations used here). The case jP for $j=1,2$ corresponds to $n=2,3$ respectively and one computes $\tau_j=\infty$ from Eq:9 and hence $\tau_{R^*}=\infty$ from Eq:12; the system goes through n steps and then remains ''indefinitely'' active (see above about thermal decay). Thus the CV of E^*_{area} and I_{area} in Table 1 and Table S1 in the supplementary material, are not due to variations caused by R^* shutoff by Arr binding. The first case when $\tau_{R^*}<\infty$ and deactivation is possible, is the case $3P$ corresponding to $n=4$

reported in Eq:13. Going from 3P to 6P, the $\mathrm{CV}(\mathrm{E}^*_{\mathrm{area}})$ and the $\mathrm{CV}(\mathrm{I}_{\mathrm{area}})$ remain essentially the same.

To illustrate the rationale of our main results, consider mutant rhodopsin with only 3 available phosphorylation sites. Since 3 phosphates are needed for Arr binding [20], no randomness is present in the deactivation process, if randomness is only measured in terms of steps to shutoff. This suggest that the source of variability is in other components of the process. Table 1 indeed shows that if the sojourn times of R^* in each of its phosphorylation states are taken to be deterministic (Case 2), then the variability of the photoresponse is negligible. If on the other hand such sojourn times are permitted to be random, then the variability rises to experimentally observed levels (Figure 1), both for WT and genetically modified R^* with 3-5P. This should not be interpreted, however, as though the reproducibility decreases as the number $(n-1)$ of available phosphorylation sites increases. We stress that increasing n does not necessarily mean that the mean number N to R^* shutoff increases. The latter depends on the biochemistry of the process via Eq:10–Eq:11. Likewise the expected average τ_{R^*} of the random lifetime of R^* is generated by the biochemistry in Eq:7–Eq:12 and n; in particular it is different for different genetically modified mice (0P,1P,etc.). The lifetime of R^* is randomly chosen by the biochemistry in each of its random trials.

For WT mouse, and only in this case, the expected lifetime τ_{R^*} of R^*, as defined by formula Eq:9–Eq:12, coincides with the experimentally measured, effective average lifetime $\tau_{\mathrm{R;eff}}$. In [29] it is reported $\tau_{\mathrm{R;eff}} \approx 75\mathrm{ms}$ as an upper limit, whereas several recent studies [28,30,31] suggest that $\tau_{\mathrm{R;eff}}$ might be as low as 40 ms (see § **Parameters**).

Therefore, we performed all simulations for both values, which yielded very similar CVs, both functionally and numerically (Figure 1 and Tables 2–3, and Figure S1 and Tables S1,S3, in the supplementary material). These similarities suggest that reproducibility is independent of the actual value of $\tau_{\mathrm{R;eff}}$ and depends only on the functional, sequence of the deactivation cascade, as predicted by our biochemical scheme (Eq:9– Eq:12). Further remarks on these two parameters and corresponding CVs are in § **On the Parameters τ_{R^*} and ν_{RG}**.

We stress that the model includes only the deactivation mechanism due to Arr binding and does not include R^* inactivation due to other causes such as thermal decay to opsin occurring over a time course of $\approx 50\mathrm{s}$ ([13]).

In [1] the $\mathrm{CV}(\mathrm{I}_{\mathrm{area}})$ is computed over a time course of over 15 s, which is beyond the time course 0.1s of R^* inactivation. According to our scheme, based on direct biochemical measurements of arrestin binding to separated rhodopsin species

Table 3. The sequences $\nu_i\tau_i$ for the dynamics of $\tau_{\mathrm{R;eff}} \approx 75\mathrm{ms}$ and $\nu_{\mathrm{RG}} \approx 330\mathrm{s}^{-1}$.

6P (WT)	N	4.45						
	τ_{i}	15.87	19.05	23.81	10.93	12.35	14.18	16.67
	ν_{i}	330.00	200.16	121.40	73.63	44.66	27.09	16.43
	$\tau_{\mathrm{i}}\nu_{\mathrm{i}}$	5.24	3.81	2.89	0.80	0.55	0.38	0.27
5P	N	4.30						
	τ_{i}	19.05	23.81	31.75	12.35	14.18	16.67	
	ν_{i}	330.00	200.16	121.40	73.63	44.66	27.09	
	$\tau_{\mathrm{i}}\nu_{\mathrm{i}}$	6.29	4.77	3.85	0.91	0.63	0.45	
4P	N	4.15						
	τ_{i}	23.81	31.75	47.62	14.18	16.67		
	ν_{i}	330.00	200.16	121.40	73.63	44.66		
	$\tau_{\mathrm{i}}\nu_{\mathrm{i}}$	7.86	6.35	5.78	1.04	0.74		
3P	N	4						
	τ_{i}	31.75	47.62	95.24	16.67			
	ν_{i}	330.00	200.16	121.40	73.63			
	$\tau_{\mathrm{i}}\nu_{\mathrm{i}}$	10.48	9.53	11.56	1.23			
2P	N	3						
	τ_{i}	47.62	95.24	∞				
	ν_{i}	330.00	200.16	121.40				
	$\tau_{\mathrm{i}}\nu_{\mathrm{i}}$	15.71	19.06	∞				
1P	N	2						
	τ_{i}	95.24	∞					
	ν_{i}	330.00	200.16					
	$\tau_{\mathrm{i}}\nu_{\mathrm{i}}$	31.43	∞					
0P	N	1						
	τ_{i}	∞						
	ν_{i}	330.00						
	$\tau_{\mathrm{i}}\nu_{\mathrm{i}}$	∞						

The sequences ν_i (s^{-1}), τ_i(ms) and the average number N of steps to shutoff of R^*, for WT and mutant mice, computed from Eq:9–Eq:11. Computation for the dynamics of $\tau_{\mathrm{R;eff}} \approx 75\mathrm{ms}$ and $\nu_{\mathrm{RG}} \approx 330\mathrm{s}^{-1}$. The parameters τ_{R^*} and $\tau_{\mathrm{R;eff}}$ and their equivalence are discussed in § **Parameters**.

doi:10.1371/journal.pcbi.1001031.t003

with different numbers of attached phosphates ([20]), cases $0P$, $1P$ and $2P$ do not permit shutoff by Arr binding and R^* remains active much longer than the 3 s of our simulations. Thus the CV due to R^* deactivation reflects its thermal decay to opsin ([12]). In this case, shutoff is an abrupt 1-step process, implying, by Poisson statistic, CV = 1. This is essentially what is reported in [1]. For the cases $5P$ and $6P$, although the experiments of [1] are carried over a time course of 15 s the $CV(I_{area})$ is essentially due to shutoff by arrestin binding, which occurs within a time course of 0.1 s, whereas decay to opsin is much slower. Considering the slow rate of thermal inactivation of rhodopsin, the probability of thermal decay within the first 0.1 s is negligible relative to the probability of decay due to Arr binding. Accordingly, the $CV(I_{area})$ reported in [1] for $5P$ and $6P$ is similar, as we find. The crucial cases $3P$ and $4P$ were not measured in [1].

The CTMC scheme we propose here differs from the Poisson statistics used in [1,2], where the CV of I_{area} is claimed to be proportional to $1/\sqrt{n}$. It should be noted that the number of available sites does not coincide with the average number of steps to shutoff and that each step weighs differently in the deactivation process, due to its biochemical history.

We return briefly to the explicit, theoretical formula Eq:3, valid under the assumptions of Eq:4, and hence for the cases 3-6P. We have already remarked that its theoretical values (for **Case 1**) are in agreement with our simulations (lines 2 and 3 of Table 1). If one would artificially concoct a biochemistry by which all the products $(\nu_j\tau_j)$ are the same for all $j=1,\ldots,N$, then formula Eq:3 would give $CV(E^*_{area})=1/\sqrt{N}$. This occurrence might suggest that the CV of the photoresponse decreases as the reciprocal of the square root of the number N of steps to shutoff. A calculation from Eq:7–Eq:11, in agreement with known biochemistry ([20]), shows that the products $(\nu_j\tau_j)$ are not constant (Table 3). In addition, even if this were the case, the variability of the photocurrent is very different from that of E^*_{area}, as the relation between these functionals is highly non-linear [8,11].

A further examination of Table 3 for 3-6P, shows that in all cases (WT or mutant), only the first few steps contribute significantly to the total activity $\sum_{i=1}^{N}\nu_i\tau_i$; the remaining ones being negligible. In view of the theoretical formula Eq:3, this is further evidence that increasing the number of steps does not significantly decrease the $CV(E^*_{area})$.

In all cases (WT or mutant) we found that the diffusion of the second messengers cGMP and Ca^{2+} in the cytoplasm acts as the dominant variability suppressor, thereby confirming the results of [8] and extending the analysis to a variety of transgenic models.

These results are made possible by separating the activation/deactivation module from the transduction module. In addition, in the activation/deactivation module, one further separates the biochemical effects of each phosphorylation contributing to the responses, thereby allowing an examination of the role of the underlying biochemistry during R^* deactivation. Incorporating the sequence of biochemical steps, described in **Methods**, allowed us to recapitulate experimental results qualitatively and quantitatively (Figure 2). It is worth noting that with realistic biochemistry, where Arr acquires a high binding affinity after 3 phosphorylation steps [20], the number of inactivation steps actually involved in shutting down individual SPRs varies very little. Therefore the fact that this number contributes virtually nothing to SPR variability, is one of the mechanisms maintaining the reproducibility of SPR.

Methods

The Mathematical CTMC Model

The state diagram of the CTMC describing R^* deactivation by Rhodopsin Kinase (RK) phosphorylating the C-terminal serines and threonines in rhodopsin, is shown in Figure 3 with circles and arrows denoting states and transitions respectively.

The states are labeled by the indices $i=1,\ldots,n+1$, and the transitions between connected states are labeled by transition rates λ_i and μ_i. The R^* catalytic activity in its $i-$th state is ν_i. The number n of phosphorylation levels is determined by the number $n-1$ of phosphorylation sites of rhodopsin, which varies in different species. In mouse, rhodopsin has six phosphorylation sites [3]. State 1 is the non-phosphorylated level, representing newly activated rhodopsin with catalytic activity ν_1; the state $(n+1)$ represents fully deactivated rhodopsin with catalytic activity $\nu_{n+1}=0$; states 2 to n represent different phosphorylation levels, in which rhodopsin holds $n-i$ sites available for phosphorylation, with $(i-1)$ sites already phosphorylated, and has catalytic activity ν_i. The states 1 to n are active states and the state $(n+1)$ is the inactive state. Specifically for WT mouse, there are seven $(n=7)$ active states, including state 1 where R^* is active and not phosphorylated. Transitions between active states are governed by the phosphorylation rates λ_i. For notation consistency, we let $\lambda_n=0$. Transitions between active states and the inactive state are governed by the arrestin binding rates μ_i. Arrestin binds with high affinity only to phosphorylated rhodopsin [20,26,32,33], therefore, $\mu_1=0$.

A newly isomerized rhodopsin is in state 1. It undergoes a random number of phosphorylations before it transitions to the fully deactivated state $(n+1)$. A rhodopsin with $(n-1)$ available phosphorylation sites could be phosphorylated at most $(n-1)$ times to state n. Generally, in state $i=1,\ldots,n-1$, rhodopsin either interacts with rhodopsin kinase adding one more phosphate and transitions to the next phosphorylation level with a rate of λ_i, or it binds arrestin which quenches its catalytic activity, and transitions to the inactive state with a rate of μ_i. This process is a Bernoulli trial with the probability of a further phosphorylation given by $\frac{\lambda_i}{\lambda_i+\mu_i}$ and the probability of arrestin binding given by $\frac{\mu_i}{\lambda_i+\mu_i}$. This statistical scheme permits one to model rhodopsin deactivation also in transgenic animals with different number of rhodopsin phosphorylation sites. For example, if $1\le m\le n-1$ of the $(n-1)$ phosphorylation sites are mutated, we could set

$$\lambda_{i-1}=0, \quad \text{and} \quad \mu_i=0, \text{for} \quad i=n-m+1,\ldots,n$$

to reflect the effect of the mutation. It should be pointed out that, given m mutated sites, the model removes any m of the available

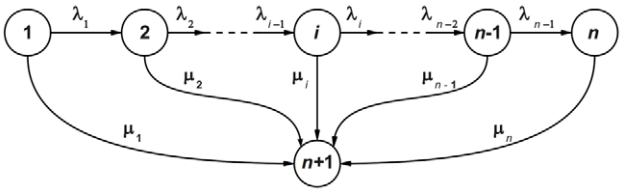

Figure 3. State diagram of CTMC model for rhodopsin deactivation. States 1 to n are active states and state n+1 is the inactive state. The phosphorylation rates and arrestin binding rates are denoted respectively by λ_i and μ_i.
doi:10.1371/journal.pcbi.1001031.g003

sites with no discriminating criterion such as their ordering on the C-terminus. Although the phosphorylation of different sites in WT rhodopsin apparently proceeds in some order [34], the overall number of rhodopsin-attached phosphates, rather than their positions on the C-terminus, determines arrestin binding [3,20,35]. Accordingly, the model treats them as equal by attributing them the same biochemical function of holding a phosphate.

Let P_i denote the probability that a single R^* is in the state i. Then the mathematical description of the CTMC model shown in Figure 3 is [14,15]

$$\begin{aligned} \dot{P}_1 &= -(\lambda_1+\mu_1)P_1, && P_1(0)=1 \\ \dot{P}_i &= \lambda_{i-1}P_{i-1}-(\lambda_i+\mu_i)P_i, && P_i(0)=0 \qquad \text{for } i=2,\ldots,n \\ \dot{P}_{n+1} &= \sum_{i=1}^{n}\mu_i P_i, && P_{n+1}(0)=0. \end{aligned} \tag{5}$$

Note that the integer i used to label the state of R^* is one plus the corresponding level of phosphorylation, which is $(i-1)$. For example, the phosphorylation level 0 corresponds to state 1, and $(n-1)$ sites are phosphorylated in state n. The sojourn time s_i of R^* in state i, is taken as an exponentially distributed random variable with mean $\tau_i=\frac{1}{\lambda_i+\mu_i}$. The sequences of the phosphorylation rates by RK $\{\lambda_i\}$, the activities of Arr $\{\mu_i\}$, and the catalytic activities $\{v_i\}$, depend on the underlying biochemistry, and vary with phosphorylation levels [26,36].

The Sequence $\{v_i\}$ of Catalytic Activities of R^*

The catalytic activity v_i of R^* in the $i-$th state is the production rate of activated G protein G^* by R^*. While R^* is active in each state $i=1,\ldots,n$, including the first unphosphorylated state ($i=1$), its activity decreases with increasing phosphorylation levels. The catalytic activity of rhodopsin with different numbers of attached phosphates was experimentally measured by Wilden [26]. In this study differentially phosphorylated rhodopsin species were actually separated, so the conclusions were based on direct measurements and did not involve untested assumptions. Although similar conclusions were later reached by Gibson et al. [32], these authors did not separate differentially phosphorylated rhodopsin species, using preparation with different average phosphorylation levels instead. Their calculations are based on the assumption of Poisson distribution of rhodopsin species with different number of phosphates ([32]). This does not appear realistic, considering the distribution determined by rhodopsin fractionation ([26,33]). Therefore, our model assumes that the binding affinity of phosphorylated R^* for G^* decreases exponentially with each added phosphate. Thus, based on data published by Wilden [26], we assume

$$v_i=v_{RG}e^{-k_v(i-1)}, \qquad i=1,...,n, \tag{6}$$

where $v_{RG}=v_1$ is the catalytic activity of R^* in its initial, unphosphorylated state, and k_v is positive. The value of v_{RG} in Eq:6 has been extracted from the published data after an extensive consistency and sensitivity analysis ([37]). The parameters v_{RG} and k_v are linked and subject to mutual limitations. It has been shown that in arrestin knockout mice, the initial kinetics of single photon response deactivation closely resembles that of WT, whereas the later phase of deactivation is abrogated (Xu et al., 1997). Initial deactivation is attributable to rhodopsin phosphorylation, which is preserved in these animals. Then deactivation stops at about 50% of the peak current suppression, and remains essentially steady thereafter. This level of current drop reflects the ability of fully phosphorylated mouse rhodopsin to activate transducin, corresponding to the catalytic activity v_7 when all 6 sites are phosphorylated. Thus from Eq:6 one has $v_7=v_{RG}e^{-6k_v}$. Mutual calibration of v_{RG} and k_v is discussed in the section on parameters. Here we stress that they are determined from experimental data for both WT and mutant mice, and not chosen by fitting.

Phosphorylation Rates $\{\lambda_i\}$ and Affinity of R-RK

While the explicit dependence of R^*-RK binding affinity and the R^* phosphorylation rates on the various biochemical states is not known, there is qualitative biochemical support for the notion that R^*-RK affinity decreases systematically with the phosphorylation level of R^* [38]. It is shown in Buczylko et al. [39], that phosphorylated RK has significantly lower ability to phosphorylate already phosphorylated R^* than unphosphorylated R^*. Moreover, Mendez et al. [3] showed that the rate of R^* deactivation depends not on the identity of the available sites, but on their total number. We used the biochemically realistic assumption that the rate of phosphorylation is proportional to the number of serines and threonines still available for RK on the rhodopsin molecule. Mechanistically this means that the probability that upon binding to light-activated rhodopsin RK dissociates without adding another phosphate increases with the number of phosphates present, reaching 1 when all six sites are already phosphorylated. This assumption is consistent with in vivo observations by Mendez et al [3] that the removal of even one or two rhodopsin phosphorylation sites slows down photoresponse inactivation. Note that λ_i is the rate at which RK phosphorylates R^* in its $i-$th state. It depends on the on-rate of RK binding to R^* in this state, and the rate of phosphate transfer, which were never separated experimentally and were not separated in our model.

We set the sequence $\{\lambda_i\}$ as linearly decreasing by increasing phosphorylation levels, that is the phosphorylation rate is proportional to the total number of the available sites and is independent of their biochemical identity. Thus

$$\lambda_i=(n-i)\lambda_o \qquad \text{for } i=1,\ldots,n \tag{7}$$

where λ_o is a rate constant, discussed and calibrated in the section on parameters. Formula Eq:7 can be arrived at by postulating that RK has a fixed affinity for binding to R^* and that each of the phosphorylation sites could be occupied with an equal rate λ_o. Therefore R^* phosphorylation rate depends on the number of phosphorylation sites available for RK. Since R^* in state i has $n-i$ available phosphorylation sites it has a phosphorylation rate $(n-i)\lambda_o$. Note that this model, similar to previously proposed ones, is based on the assumption that a single site is phosphorylated as a result of each rhodopsin encounter with RK. This assumption has not been experimentally tested.

Arr Binding Rate $\{\mu_i\}$ and Affinity of R-Arr

Arrestin binding ensures the timely termination of R^* signaling, and it depends on the R^*-Arr affinity. Several studies [26,32,36], suggest that arrestin affinity increases with increasing phosphorylation levels. Note that only the "irreversible" binding that terminates rhodopsin activity is taken into account here; that is the binding which occurs with high enough affinity to make the complex half-life much greater than the time course of the SPR. In a recent study, Vishnivetskiy et al. [20] found that unphosphorylated and mono-phosphorylated R^* show the same low Arr binding levels. In particular, a single receptor-attached phosphate

does not facilitate Arr binding; two are necessary to induce higher affinity interaction, and R^* with three phosphates is fully capable of binding Arr with the affinity that makes the interaction essentially irreversible on the time scale of the SPR. Moreover, higher phosphorylation levels do not increase the stability of Arr complex with light-activated rhodopsin [20]. Based on the data in [20], we set the sequence $\{\mu_i\}$ for Arr binding rate by the phosphorylation level as

$$\mu_1=\mu_2=\mu_3=0, \quad \mu_i=\mu_o, \qquad i=4,...,n, \tag{8}$$

where μ_o is the Arr binding rate when Arr affinity reaches its maximum after several phosphorylations. Note that n in the model describes arrestin binding that terminates transducin activation. Thus, it reflects the rate of formation of arrestin-rhodopsin complexes that are stable enough to survive significantly longer than the time course of a single photon response analyzed here. Since the stability of arrestin complex with unphosphorylated and mono-phosphorylated rhodopsin is much lower [20,40–42], allowing for arrestin dissociation and consequent rhodopsin reactivation within this time, we set $\mu_1=\mu_2=0$. Since $\mu_1=\mu_2=0$, R^* in states $i=1,2$ surely transitions to the states $i=2,3$ respectively. The data in vivo [3] and in vitro [20] also suggest that two rhodopsin-attached phosphates are not sufficient to induce Arr binding with high enough affinity for rapid deactivation. Therefore, we set $\mu_3=0$.

The effect of the level of rhodopsin phosphorylation on arrestin binding was explored in two studies. Gibson et al [32] concluded that arrestin affinity linearly increases with the level of phosphorylation in the range of 1–4 phosphates per rhodopsin. The authors used preparations of phosphorylated rhodopsin in native disc membranes that are well known to be highly heterogeneous, containing rhodopsin species carrying from zero to seven phosphates (bovine rhodopsin has seven RK phosphorylation sites) [26,43]. The authors attempted to solve this problem by using several assumptions (that were not experimentally tested) to compute the fraction of rhodopsin molecules with different phosphorylation levels as a function of average phosphorylation, which was the only parameter actually measured [32]. The authors calculations were based on an additional assumption that unphosphorylated rhodopsin does not bind arrestin, even though specific low affinity binding of wild type arrestin to light-activated unphosphorylated rhodopsin in vitro [40,41], and its role in inactivation of unphosphorylated rhodopsin in vivo [12,23,42] was shown. Arrestin binding in this study was measured using "extra Meta II" assay developed by Schleicher et al in 1989 [44]. This assay is based on the stabilization of active Metarhodopsin II state by bound arrestin. The most significant drawback of this assay is that it does not work above 15°C. At physiological temperatures extra Meta II is not detectable, even though it is obvious that arrestin effectively quenches rhodopsin signaling in mammals at 37°–39°C. In another study Vishnivetskiy et al [20] separated rhodopsin species with different levels of phosphorylation by chromatofocusing. Importantly, the authors quantitatively determined the presence of particular phospho-rhodopsin species in each fraction by mass-spectrometry of proteolytically removed rhodopsin C-terminus [34], obviating the need for calculations based on untested assumptions. Moreover, the binding assay in this study was performed at physiological temperature, 37°C. Based on their data, Vishnivetskiy et al concluded that arrestin demonstrates the same low affinity for rhodopsin carrying zero and one phosphate. The presence of two phosphates somewhat increases arrestin affinity, whereas arrestin binds rhodopsin with three, four, five, and six phosphates with the same high affinity, forming physiologically relevant long-lived complexes with stability sufficient for reliable quenching without possibility of reactivation on the time scale of the photoresponse [20]. These conclusions are in remarkable agreement with the work of Mendez et al in genetically modified mice expressing rhodopsin with different number of phosphorylation sites [3]. The authors of this study found that in vivo light activation of rhodopsin carrying zero, one, or two phosphorylation sites yields responses that last for many seconds, whereas rhodopsin carrying three or more phosphorylation sites is inactivated by wild type arrestin with sub-second kinetics [3]. Therefore, we based the modeling on the conclusions of these two studies [3,20]. The parameters μ_o and λ_o appearing in Eq:7–Eq:8 are calibrated by WT and mutant experimental data, and not by fitting (see section on parameters).

Random Sojourn Times $\{s_i\}$ and Random Steps to R^* Shutoff

In the state i, R^* maintains its catalytic activity v_i for a random time s_i, until further phosphorylation or Arr binding. The sojourn times s_i, for $i=1,\ldots,k\le n$ are exponentially distributed random variables with mean τ_i. The average lifetime $\tau_{R^*}(k)$ of R^* being deactivated after k random biochemical states visited by R^* before quenching, and is the sum of the τ_i up to k. Thus

$$\tau_i=\frac{1}{\lambda_i+\mu_i} \quad \text{and} \quad \tau_{R^*}(k)=\sum_{i=1}^{k}\tau_i. \tag{9}$$

Hence τ_i and τ_{R^*} are determined by the biochemistry of the process through the sequences $\{\lambda_i\}$ and $\{\mu_i\}$.

The number $1\le k\le n$ of steps after which R^* binds to Arr is itself a random variable X. The probability of R^* shutoff in k steps, or equivalently the probability of R^* undergoing $k-1$ steps of phosphorylation and a final step for Arr binding, is

$$P(X=k)=\begin{cases}0 & \text{if } n=1 \text{ (no phosphorylation sites)}\\ \dfrac{\mu_k}{\lambda_k+\mu_k}\prod_{i=1}^{k-1}\dfrac{\lambda_i}{\lambda_i+\mu_i} & \begin{cases}\text{for } n\ge 2 \text{ and}\\ \text{for } k=2,\ldots,n.\end{cases}\end{cases} \tag{10}$$

The mean steps of R^* shutoff, or equivalently the expected value of the first moment of X, is denoted by N and is given by

$$N=\sum_{k=1}^{n}kP(X=k). \tag{11}$$

Thus N is the mean of the discrete valued random variable $k\in\{1,\ldots,n\}$.

The lifetime $\tau_{R^*}(k)$ of R^* is itself a random variable with expected value

$$\tau_{R^*}=\sum_{k=1}^{n}\tau_{R^*}(k)P(X=k). \tag{12}$$

These remarks permit one to detect the pattern of the means τ_j of the random sojourn times s_j. First, the expected lifetime $\tau_{R^*}(\ell P)$ of R^*, as a function of the number ℓ of available phosphorylation sites, decreases with increasing ℓ; second, the sojourn times s_j, while increasing in number, each have a smaller mean τ_j. For example for 3P ($n=4$), from Eq:7–Eq:9, and Eq:10–Eq:11, one computes

$$\tau_1=\frac{1}{3\lambda_o},\quad \tau_2=\frac{1}{2\lambda_o},\quad \tau_3=\frac{1}{\lambda_o},\quad \tau_4=\frac{1}{\mu_o},$$
$$N=4;\quad \tau_{R^*}(3P)\approx 0.19s. \tag{13}$$

We stress that the number $n-1$ of available phosphorylation sites does not coincide with the mean number N of steps to R^* quenching. The number n is fixed by the structure of rhodopsin, whereas N depends on the biochemistry, through the probabilities $P(X=k)$.

Numerical Procedures and Methods

The dynamics of R^* during deactivation is analyzed by the CTMC model in Eq:5, which is numerically integrated in the Matlab platform. Its output is integrated into the spatio-temporal model and its Matlab code introduced in [8,11]. This produces pointwise values of the effector $[E^*]$, [cGMP] and $[Ca^{2+}]$ on the ROS and permit one to compute the current response $j_{tot}(t)$ as a function of time and thus the functionals of effector and current in Eq:1–Eq:2.

Simulations were performed for each of the 3 Test Cases. Random numbers are generated according to the exponential distribution of the random sojourn times s_i, for each of wild type, transgenic and Arr knock-out cases indicated above. The corresponding R^* dynamics is computed and the functionals in Eq:1–Eq:2 are evaluated. For each case, after about 5,000 numerical simulations, we compute the mean, the standard deviation and the coefficient of variation (CV) of these functionals.

For WT mice the sequences $\{\lambda_i\}$ and $\{\nu_i\}$ are chosen as in Eq:6–Eq:7. For mice lacking phosphorylation whether by COOH-terminal truncations ([24,25]) or RK knockout ([1,3]), in the CTMC one sets $n=1$ in Eq:5 and $\mu_1=0$, so that R^* would remain in state 1 with catalytic activity ν_1 for the whole process. If $1\le m\le 6$ of the six phosphorylation sites are mutated out, we would have a CTMC model with $n=7-m$. For mice lacking Arr ([24]), we let $\mu_i=0$, for $i=1,...,7$ in the CTMC model in Eq:5.

Parameters

In [37], we have generated a complete, self-consistent set of parameters for the mouse rod phototransduction, calibrated by least square fitting of the model in [8,9,11]. to a set of experimental data kindly provided Dr. C. Makino, leading to Table S2 (Text S1). Note that these parameters describe SPR recorded in Locke's solution used in [3,7,24,25,28,29,42,45–49], rather than in Ames' solution used in [1,2]. For reasons that remain to be elucidated, the latter has greater amplitude and duration, although the recovery in both conditions is rate-limited by transducin inactivation ([28]).

Figure 4 compares the simulated SPR by our model with the parameters of Table S2, and the experimental SPR kindly provided by C. Makino. The new parameters involved in the present investigation are the biochemical sequences $\{\nu_i\}$, $\{\lambda_i\}$ and $\{\mu_i\}$. Below we indicate in detail how they have been determined. Their estimated values are reported in Table 4. Given the catalytic rate ν_{RG} the sequence $\{\nu_i\}$ is determined from Eq:6 whence the rate k_ν is known.

Estimate of k_ν. In the experiments of [26] a large pool of G proteins, PDE and cGMP was mixed with a large quantity of rhodopsin R_i with a known number $(i-1)\in\{1,\dots,6\}$ of phosphates. Then the R_i were activated by a brief flash of light to produce a number of isomerizations Φ_i per μm^3, and the rate of depletion cGMP was recorded. Since only three purified proteins are present in this assay, rhodopsin, transducin, and PDE, rapid inactivation mechanisms present in vivo do not operate. Therefore, the number of activated transducin molecules is proportional to the number of light-activated rhodopsins and their activity, and the number of active PDE molecules is proportional to the number of active transducins and does not change in time.

The number of molecules involved, all in the same environment, is so large as to justify a lumped description of the phenomenon by means of standard balance equations

$$\frac{d}{dt}[\mathrm{cGMP}]=-k_{hyd}[E^*][\mathrm{cGMP}] \tag{14}$$

where $[E^*]$ is the number of molecules of fully activated PDE per μm^3, and k_{hyd}, in $\mu m^3 s^{-1}$ is the rate of hydrolysis of cGMP by E^*. If Φ_i is sufficiently large, the system saturates in the sense that all available molecules of PDE are fully activated. Denoting by $[E^*]_{sat}$ the limiting saturation, one computes

$$[E^*]_{sat}=\nu_i\Phi_i/k_E$$

where ν_i is the activity of R^* in its $i-$th state, and k_E is the decay rate of E^*. It is assumed that for large Φ_i the time to saturation is very small so that, in Eq:14, one approximates $[E^*]\approx[E^*]_{sat}$. from the second of Eq:14. These remarks in Eq:14 imply

$$\frac{d}{dt}[\mathrm{cGMP}]_i\approx-\frac{k_{hyd}}{k_E}\nu_i\Phi_i[\mathrm{cGMP}]_i \tag{15}$$

Table 4. CTMC model parameters.

Symbol	Units	Definition	Value		References
λ_o	s^{-1}	Rhodopsin phosphorylation rate	*10.5*	**19**	computed as in **Determining the Sequences $\{\lambda_i\}$ and $\{\mu_i\}$**
μ_o	s^{-1}	Arresting binding rate	*60*	**120**	computed as in **Determining the Sequences $\{\lambda_i\}$ and $\{\mu_i\}$**
k_ν	-	Decay constant of catalytic activity of R*	*0.5*	**0.5**	[26]
$\tau_{R;eff}$	ms	Average lifetime of active R*	*75*	**41**	[*29*], [**28,30,31**]
N	-	Average number of steps of active R* before shut off	*4.45*	**4.41**	computed from Eq:9–Eq:11

Italic: $\tau_{R;eff}\approx 75$ *ms*. **Bold:** $\tau_{R;eff}\approx 41$ **ms**. The parameters τ_{R^*} and $\tau_{R;eff}$ and their equivalence are discussed in § **Parameters**.
doi:10.1371/journal.pcbi.1001031.t004

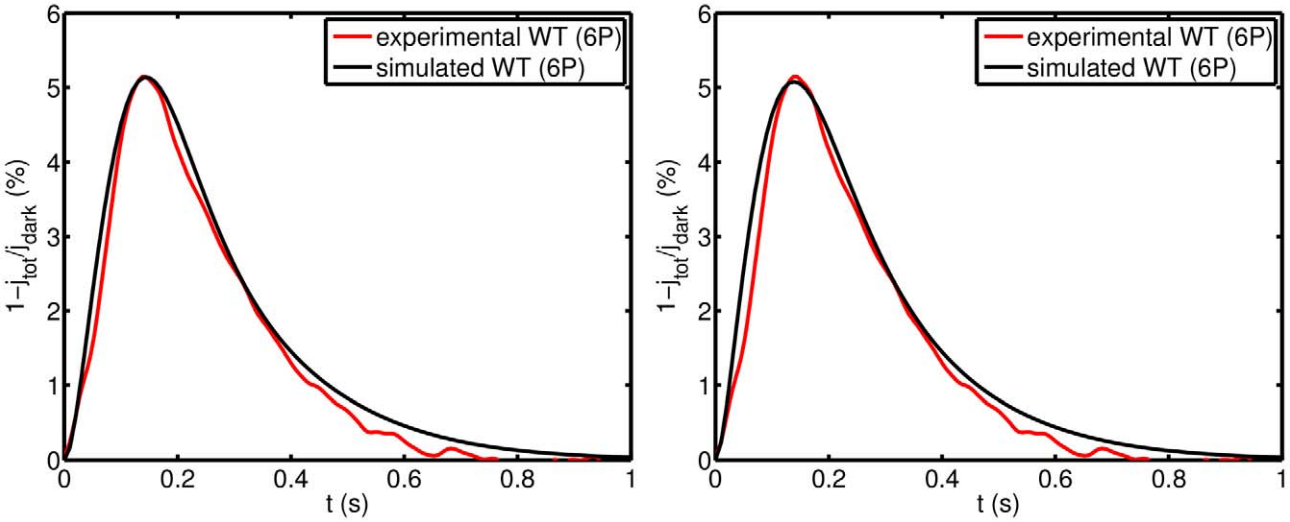

Figure 4. Mouse SPRs by simulation (black) and experiment (red). The simulation is conducted with the parameters shown in Table S2 for the dynamics $\tau_{R;eff} \approx 75$ms and $\nu_{RG} \approx 330 s^{-1}$ (left), and the dynamics suggested in [28,30,31](right). **Left**: Dynamics of $\tau_{R^*} \approx 75$ms and $\nu_{RG} \approx 330 s^{-1}$. The WT SPR exhibits a maximum of 5.13%, decrease of current at 0.14s after activation. Experimental data is an average of sets of SPRs kindly provided by C. Makino. **Right**: Same experimental (red) and simulated (black) WT response with $\tau_{R^*} \approx 41$ms and $\nu_{RG} \approx 575 s^{-1}$. Experimental data kindly provided by C. Makino.
doi:10.1371/journal.pcbi.1001031.g004

where the indexed $[cGMP]_i$ signifies that in principle the solution of such equation depends on the activity of the $i-$th phosphorylation state of R^*. At saturating light levels the rates $[cGMP]_i'$ reach a limiting value independent of i. Moreover at such limiting rates the $[cGMP]_i$ are essentially the same for all i, since they are hydrolyzed by $[E^*]_{sat}$. It is reported in [26] that the same rate of depletion $[cGMP]_1'$ for an experiment with rhodopsin R_1 (no phosphates) with activity $\nu_1 = \nu_{RG}$, and number of isomerizations Φ_1, can be obtained from an experiment with rhodopsin R_7 (6 phosphates), and catalytic activity ν_7, provided the number of isomerizations Φ_7 is 10 times larger than Φ_1. Equation Eq:15 with these data and indicated assumptions yields

$$1 = \frac{[cGMP]_7'}{[cGMP]_1'} \approx \frac{k_{hyd}\nu_7\Phi_7[cGMP]}{k_{hyd}\nu_1\Phi_1[cGMP]} = \frac{10\nu_7}{\nu_{RG}}.$$

From this and Eq:6 one computes $10 = e^{k_\nu 6}$ or $k_\nu \approx 0.38$.

Determining the sequences $\{\lambda_i\}$ and $\{\mu_i\}$. The modeling assumptions contained in Eq:7–Eq:8 reduce these sequences to the determination of λ_o and μ_o. These are constrained by Eq:12. Therefore, if the expected lifetime τ_{R^*} of activated rhodopsin, given by Eq:12, is experimentally estimated, then only one of these parameters, λ_o or μ_o, is independent. When τ_{R^*} is fixed at a particular value, the remaining free parameter is estimated against the experimental results of [24] for SPR in transgenic mice lacking arrestin, as follows. In the absence of arrestin, the activated rhodopsin gets phosphorylated from one level to another until all its six sites are occupied. Its activity is reduced with phosphorylation, and kept fixed after the last phosphorylation, for the remainder of the process. Such activity causes the response tail to maintain almost a half of its peak value (Figure 2C,D). Thus λ_o and μ_o are constrained by Eq:8 and by the requirement that putting $n = 7$ in the CTMC Eq:5 and $\mu_i = 0$ for all $i = 1, \ldots, 7$ the time asymptotic current suppression is about $\frac{1}{2}$ of the peak current suppression.

It is worth stressing that the parameter calibration has been effected by enforcing at the same time, the WT response, the response of transgenic mice lacking arrestin, and by linking the rates λ_i and μ_i to the experimental value of τ_{R^*} by Eq:12. It is also worth noting that here we simulated the first 3 s of the photoresponse. Light-activated rhodopsin can also be inactivated in an RK- and Arr-independent manner via thermal decay to opsin with very low activity towards transducin. Since this process is very slow, with half-life of ~ 49 s in mouse photoreceptors [13], we did not take it into account in our modeling.

On the parameters τ_{R^*} and ν_{RG}. In Table S2, $k_R \approx 13.3$s is the reciprocal of the experimental value of the average lifetime of R^* for WT mouse, denoted by $\tau_{R;eff}$, and determined as the time constant of an exponential decay function used to approximate R^* lifetime ([28,30,31]). As such $\tau_{R;eff}$ is an "effective lifetime". In [29] $\tau_{R;eff} \approx 75$ms is an upper limit of R^* lifetime.

The expected value τ_{R^*} of R^* lifetime given by Eq:12 is the average of the times it takes R^* to be quenched after k steps, weighted by the probabilities of quenching after k steps. This number depends only on the biochemistry defined by the sequences $\{\nu_i\}$ and $\{\lambda_i\}$.

If one knew these sequences a-priori, no knowledge of $\tau_{R;eff}$ would be needed. The numerical value of the latter is used to generate an extra link between the parameters λ_o and μ_o, for WT mouse ($n = 7$) to reduce the number of free parameters. Thus the underlying assumption is that for WT mouse, the expected value τ_{R^*} of the random variable $\tau_{R^*}(k)$ is *numerically* comparable with the experimentally measured numerical value of $\tau_{R;eff}$, and thus one sets *numerically* $\tau_{R^*} = \tau_{R;eff}$. For this reason, when referring to WT mouse, and only in this case, we use τ_{R^*} and $\tau_{R;eff}$ interchangeably. However for genetically modified mice ($n < 7$) the expected values of τ_{R^*} given by formula Eq:13 differ from $\tau_{R;eff}$.

It should be pointed out however that τ_{R^*} is a derived parameter through formula Eq:12. It is the biochemistry that determines τ_{R^*} through the RK on-rates λ_i and the Arr on-rates μ_i. Thus τ_{R^*} changes in genetically modified mice according to the number of mutated sites, and the resulting biochemistry.

Several recent studies give a lower estimate $\tau_{R;eff} \approx 40ms$ for WT [30]. Because of the importance of this parameter we have reproduced our simulations also for $\tau_{R;eff} \approx 41ms$, and found no appreciable difference in the numerical values or the general pattern of the resulting variability functionals (see Figure S1 and Tables S1, S3 of the supplementary material). Thus, the functional conclusions of this study do not depend on the numerical value of $\tau_{R;eff}$.

By taking a shorter $\tau_{R;eff}$, the SPR for WT mouse can be reproduced by imposing a larger catalytic rate $\nu_{RG} \approx 575s^{-1}$ (i.e., activation of transducin by rhodopsin every 2 ms). A few other parameters have been slightly modified the most noticeable of which are the RK on-rate λ_o and the Arr on-rate μ_o. Using the pair $\tau_{R;eff} \approx 75ms$ and $\nu_{RG} \approx 330s^{-1}$ and computing λ_o and μ_o as indicated in the previous section, one estimates $\lambda_o \approx 10.5s^{-1}$ and $\mu_o \approx 60s^{-1}$. Using the pair $\tau_{R;eff} \approx 41ms$ and $\nu_{RG} \approx 575s^{-1}$, one estimates $\lambda_o \approx 19s^{-1}$ and $\mu_o \approx 120s^{-1}$. All the indicated simulations have been run for both sets of parameters with no appreciable difference in the results (Figure 1 and Tables 2–3, and Figure S1 and Table S1,S3 in the supplementary material).

The value of ν_{RG} reported in Table S2 corresponds to the value ν_{RG1} as calculated from Eq:6 for $i=1$. The (random) production of G^* by R^* in its $i-th$ state is $\nu_i s_i$. If shutoff occurs in k steps, the average activity over these steps is

$$\nu_{RG}(k) = \frac{1}{\tau_{R^*}(k)} \sum_{i=1}^{k} \nu_i \tau_i. \tag{16}$$

This is a random variable whose expectation is the expected (average) activity $\nu_{RG;av}$ of the process

$$\nu_{RG;av} = \sum_{k=1}^{n} \nu_{RG}(k) P(X=k). \tag{17}$$

A calculation for 6P and $\tau_{R;eff} \approx 75ms$ gives $\nu_{RG;av} \approx 174s^{-1}$. This value is within the published range of average R^* activity as discussed in [37]. A similar calculation for 6P and the faster dynamics $\tau_{R;eff} \approx 41ms$ gives $\nu_{RG;av} \approx 307s^{-1}$.

Remaining in the context of WT mouse, the shortening of $\tau_{R;eff}$ from 75ms to 40ms forces a faster dynamics so that the total activity remains unchanged. One verifies that the activity $\tau_{R;eff}\nu_{RG;av}$ remains the same for both values of $\tau_{R;eff}$. The two dynamics generate two different biochemical sequences, say for example

$$\{\lambda_{1,i}, \nu_{1,i}, \tau_{1,i}\}, \quad \text{and} \quad \{\lambda_{2,i}, \nu_{2,i}, \tau_{2,i}\}.$$

An examination of Table 3 and Table S3 in the supplementary material reveals that, for each fixed i the products $\nu_{1,i}\tau_{1,i}$ and $\nu_{2,i}\tau_{2,i}$, are essentially the same for the two dynamics. Thus the total R^* activity is redistributed in "equal bits", although in different time intervals $\tau_{1,i}$ and $\tau_{2,i}$, and different catalytic activities $\nu_{1,i}$ and $\nu_{2,i}$. The theoretical formula Eq:3 then gives

$$\begin{aligned} CV(E^*_{area}, \text{for } \tau_{R;eff} \approx 75ms) &= \frac{\sqrt{\sum_{j=1}^{N} (\nu_{1,j}\tau_{1,j})^2}}{\sum_{j=1}^{N} \nu_{1,j}\tau_{1,j}} \\ &\approx \frac{\sqrt{\sum_{j=1}^{N} (\nu_{2,j}\tau_{2,j})^2}}{\sum_{j=1}^{N} \nu_{2,j}\tau_{2,j}} \\ &= CV(E^*_{area}, \text{for } \tau_{R;eff} \approx 40ms) \end{aligned}$$

This explains why the CVs of E^*_{area}, and hence those of I_{area} are so similar, for each of these dynamics. A further examination of Table 3 and Table S3 of the supplementary material shows that to the total activity $\sum_{i=1}^{N} \nu_i \tau_i$ contribute essentially only the first few steps, the remaining ones being negligible. In view of the theoretical formula Eq:3, this is further evidence that increasing the number of steps, does not significantly decrease the $CV(E^*_{area})$.

The main difference between the CVs in Table 1 and Table S1 in the supplementary material occurs for the pointwise functionals $E^*(t^*_{peak})$ and $I(t_{peak})$, which depend on a point evaluation at t^*_{peak} and t_{peak} respectively, and do not depend on the total, integral activity up to time t.

The average number of steps to shutoff. This number is computed from Eq:10–Eq:11, and therefore it is not expected to be an integer.

For $\tau_{R;eff} \approx 75ms$ and $\nu_{RG} \approx 330s^{-1}$ and the corresponding λ_o and μ_o, one estimates $N \approx 4.45$. For the faster dynamics $\tau_{R;eff} \approx 41ms$, and $\nu_{RG} \approx 575s^{-1}$, one estimates $N \approx 4.41$.

The parameters of Table S2 and Table 4 have been slightly calibrated to satisfy simultaneously all the indicated constraints. Figure 4 compares the simulated and experimental single photon response in WT mouse. The simulations for transgenic mouse in Figure 2 are compared with the experimental data of [1,3,23–25]. The dynamics of the WT mouse SPR reported in [1], is, in absolute time, slower than that reported in [3,23–25]. The difference might be the result of using different solutions for single cell recording [2,28]. The underlying mechanism of this phenomenon remains unknown. To achieve a functional comparison with all these contributions we have reported our simulations in units of t_{peak} and likewise we have rescaled the graphs reported in [3,23] in units of their own t_{peak}. The output (given in pA in the original papers) has been rescaled in relative current suppression $1-j_{tot}/j_{dark}$.

Supporting Information

Figure S1 Comparing the CVs of the total activated effectors at time t with the CVs of the total relative charge up to time t.
Found at: doi:10.1371/journal.pcbi.1001031.s001 (0.05 MB PDF)

Figure S2 Simulations SPR for mutant phosphorylation sites of R* or with Arr knockout.
Found at: doi:10.1371/journal.pcbi.1001031.s002 (0.08 MB PDF)

Table S1 CVs of effector and current for WT and mutant mouse SPR.
Found at: doi:10.1371/journal.pcbi.1001031.s003 (0.04 MB PDF)

Table S2 Parameter table for WT SPR.
Found at: doi:10.1371/journal.pcbi.1001031.s004 (0.06 MB PDF)

Table S3 Table of distribution of activities for WT and mutant mouse SPR.
Found at: doi:10.1371/journal.pcbi.1001031.s005 (0.03 MB PDF)

Text S1 References.
Found at: doi:10.1371/journal.pcbi.1001031.s006 (0.04 MB PDF)

Acknowledgments

This work has been conducted in part using the resources of the Advanced Computing Center for Research and Education at Vanderbilt University, Nashville, TN. We thank Dr. Clint Makino, for mouse electrophysiological data.

Author Contributions

Conceived and designed the experiments: ED. Performed the experiments: GC LL. Analyzed the data: GC PB DA VVG HEH ED. Contributed reagents/materials/analysis tools: GC PB. Wrote the paper: ED. Directed the investigation: ED.

References

1. Doan T, Mendez A, Detwiler P, Chen J, Rieke F (2006) Multiple phosphorylation sites confer reproducibility of the rod's single-photon responses. Science 313: 530–533.
2. Doan T, Azevedo W, Hurley J, Rieke F (2009) Arrestin competition influences the kinetics and variability of the single-photon responses of mammalian rod photoreceptors. J of Neurosci 29: 11879–11867.
3. Mendez A, Burns ME, Roca A, Lem J, Wu LW, et al. (2000) Rapid and reproducible deactivation of rhodopsin requires multiple phosphorylation sites. Neuron 28: 153–164.
4. Field GD, Rieke F (2002) Mechanisms regulating variability of the single photon responses of mammalian rod photoreceptors. Neuron 35: 733–747.
5. Whitlock GG, Lamb TD (1999) Variability in the time course of single photon responses from toad rods: termination of rhodopsin's activity. Neuron 23: 337–351.
6. Rieke F, Baylor DA (1998) Origin of reproducibility in the responses of retinal rods to single photons. Biophys J 75: 1836–1857.
7. Burns ME, Mendez A, Chen J, Baylor DA (2002) Dynamics of cyclic GMP synthesis in retinal rods. Neuron 36: 81–91.
8. Bisegna P, Caruso G, Andreucci D, Shen L, Gurevich VV, et al. (2008) Diffusion of the second messengers in the cytoplasm acts as a variability suppressor of the single photon response in vertebrate phototransduction. Biophys J 94: 3363–3383.
9. Andreucci D, Bisegna P, Caruso G, Hamm HE, DiBenedetto E (2003) Mathematical model of the spatio-temporal dynamics of second messengers in visual transduction. Biophys J 85: 1358–1376.
10. Caruso G, Khanal H, Alexiades V, Rieke F, Hamm HE, et al. (2005) Mathematical and computational modeling of spatio-temporal signaling in rod phototransduction. IEE Proc Syst Biol 152: 119–137.
11. Caruso G, Bisegna P, Shen L, Andreucci D, Hamm HE, et al. (2006) Modeling the role of incisures in vertebrate phototransduction. Biophys J 91: 1192–1212.
12. Burns ME, Mendez A, Chen CK, Almuete A, Quillinan N, et al. (2006) Deactivation of phosphorylated and nonphosphorylated rhodopsin by arrestin splice variants. J Neurosci 26: 1036–1044.
13. Shi G, Yau KW, Chen J, Kefalov VJ (2007) Signaling properties of a short-wave cone visual pigment and its role in phototransduction. J Neurosci 27: 10084–93.
14. Varadhan S (2001) Probability Theory. Providence, R.I.: AMS.
15. Gikhman I, Skorokhod A (1969) Introduction to the Theory of Random Processes. New York: Dover.
16. Reingruber J, Holcman D (2008) The dynamics of phosphodiesterase activation in rods and cones. Biophys J 94: 1954–1970.
17. Hanson SM, Francis DJ, Vishnivetskiy SA, Klug CS, Gurevich VV (2006) Visual arrestin binding to microtubules involves a distinct conformational change. J Biol Chem 281: 9765–9772.
18. Hanson SM, Gurevich EV, Vishnivetskiy SA, Ahmed MR, X S, et al. (2007) Each rhodopsin molecule binds its own arrestin. Proc Natl Acad Sci USA 104: 3125–3128.
19. Raman D, Kennedy MJ, Hurley JB, Gurevich VV (2005) Threshold mechanism of arrestin activation: two rhodopsin-attached phosphates are necessary and sufficient for high-affinity arrestin binding. In: Association for Research in Vision and Ophthalmology Annual Meeting; 1-4 May 2005; Fort Lauderdale, Florida, United States of America.
20. Vishnivetskiy SA, Raman D, Wei J, Kennedy MJ, Hurley JB, et al. (2007) Regulation of arrestin binding by rhodopsin phosphorylation level. J Biol Chem 282: 32075–32083.
21. Rieke F, Baylor DA (1998) Single photon detection by rod cells of the retina. Rev Mod Phys 70: 1027–1036.
22. Hamer RD, Nicholas SC, Tranchina D, Liebman PA, Lamb TD (2003) Multiple steps of phosphorylation of activated rhodopsin can account for the reproducibility of vertebrate rod single-photon responses. J Gen Physiol 122: 419–444.
23. Chen CK, Burns ME, Spencer M, Niemi GA, Chen J, et al. (1999) Abnormal photoresponses and light-induced apoptosis in rods lacking rhodopsin kinase. Proc Natl Acad Sci USA 96: 3718–3722.
24. Xu J, Dodd RL, Makino CL, Simon MI, Baylor DA, et al. (1997) Prolonged photoresponses in transgenic mouse rods lacking arrestin. Nature 389: 505–509.
25. Chen J, Makino CL, Peachey NS, Baylor DA, Simon MI (1995) Mechanisms of rhodopsin inactivation in vivo as revealed by a COOH-terminal truncation mutant. Science 267: 374–377.
26. Wilden U (1995) Duration and amplitude of the light-induced cGMP hydrolysis in vertebrate photoreceptors are regulated by multiple phosphorylation of rhodopsin and by arrestin binding. Biochemistry 34: 1446–1454.
27. Wen XH, Shen L, Brush RS, Michaud N, Al-Ubaidi MR, et al. (2009) Overexpression of rhodopsin alters the structure and photoresponse of rod photoreceptors. Biophys J 9: 939–950.
28. Gross P, Burns M (2010) Control of rhodopsin's active lifetime by arrestin-1 expression in mammalian rods. J Neurosci 30: 3450–3457.
29. Krispel CM, Chen D, Melling N, Chen YJ, Martemyanov KA, et al. (2006) RGS expression rate-limits recovery of rod photoresponses. Neuron 51: 409–416.
30. Burns M, Pugh EN (2009) Rgs9 concentration matters in rod phototransduction. Biophys J 97: 1538–1547.
31. Chen CK, Woodruff ML, Chen FS, Chen D, Fain G (2010) Background light produces a recoverin-dependent modulation of activated-rhodopsin lifetime in mouse rods. J Neurosci 30: 1213–1220.
32. Gibson SK, Parkes JH, Liebman PA (2000) Phosphorylation modulates the affinity of light-activated rhodopsin for G protein and arrestin. Biochemistry 39: 5738–5749.
33. Wilden U, Hall SW, Kuhn H (1986) Phosphodiesterase activation by photoexcited rhodopsin is quenched when rhodopsin is phosphorylated and binds the intrinsic 48-kDa protein of rod outer segments. Proc Natl Acad Sci USA 83: 1174–1178.
34. Kennedy MJ, Lee KA, Niemi GA, Craven KB, Garwin GG, et al. (2001) Multiple phosphorylation of rhodopsin and the in vivo chemistry underlying rod photoreceptor dark adaptation. Neuron 31: 87–101.
35. Vishnivetskiy SA, Paz CL, Schubert C, Hirsch JA, Sigler PB, et al. (1999) How does arrestin respond to the phosphorylated state of rhodopsin? J Biol Chem 274: 11451–11454.
36. Pullen N, Brown NG, Sharma RP, Akhtar M (1993) Cooperativity during multiple phosphorylations catalyzed by rhodopsin kinase: supporting evidence using synthetic phosphopeptides. Biochemistry 32: 3958–3964.
37. Shen L, Caruso G, Bisegna P, Andreucci D, Gurevich VV, et al. (2010) Dynamics of mouse rod phototransduction and its sensitivity to variation of key parameters. IET Syst Biol 4: 12–32.
38. Palczewski K, Buczylko J, Ohguro H, Annan RS, Carr SA, et al. (1994) Characterization of a truncated form of arrestin isolated from bovine rod outer segments. Protein Sci 3: 314–324.
39. Buczylko J, Gutmann C, Palczewski K (1991) Regulation of rhodopsin kinase by autophosphorylation. Proc Natl Acad Sci USA 88: 2568–2572.
40. Gurevich VV, Benovic JL (1992) Cell-free expression of visual arrestin. truncation mutagenesis identifies multiple domains involved in rhodopsin interaction. J Biol Chem 267: 21919–21923.
41. Gurevich VV, Benovic JL (1993) Visual arrestin interaction with rhodopsin: Sequential multisite binding ensures strict selectivity towards light-activated phosphorylated rhodopsin. J Biol Chem 268: 11628–11638.
42. Song X, Vishnivetskiy SA, Gross OP, Emilianoff K, Mendez A, et al. (2009) Enhanced arrestin facilitates recovery and protects rods lacking rhodopsin phosphorylation. Curr Biol 19: 700–705.
43. Wilden U, Kuhn H (1982) Light-dependent phosphorylation of rhodopsin: number of phosphorylation sites. Biochemistry 21: 3014–3022.
44. Schleicher A, Kuhn H, Hoffman KP (1989) Kinetics, binding constant, and activation energy of the 48-kda protein-rhodopsin complex by extrametarhodopsin ii. Biochem 28: 1770–1775.
45. Chen CK, Burns ME, He W, Wensel TG, Baylor DA, et al. (2000) Slowed recovery of rod photoresponse in mice lacking the GTPase accelerating protein RGS9-1. Nature 403: 557–560.
46. Makino CL, Dodd RL, Chen J, Burns ME, Roca A, et al. (2004) Recoverin regulates light-dependent phosphodiesterase activity in retinal rods. J Gen Physiol 123: 729–741.
47. Krispel CM, Chen CK, Simon MI, Burns ME (2003) Novel form of adaptation in mouse retinal rods speeds recovery of phototransduction. J Gen Physiol 122: 703–712.
48. Krispel CM, Chen CK, Simon MI, Burns ME (2003) Prolonged photoresponses and defective adaptation in rods of Gbeta5-/- mice. J Neurosci 23: 6965–6971.
49. Mendez A, Burns ME, Sokal I, Dizhoor AM, Baehr W, et al. (2001) Role of guanylate cyclase-activating proteins (GCAPs) in setting the flash sensitivity of rod photoreceptors. Proc Natl Acad Sci USA 98: 9948–9953.